

Charge Detection in an Array of CMOS Quantum Dots

Emmanuel Chanrion,^{1,*} David J. Niegemann,¹ Benoit Bertrand,² Cameron Spence,¹ Baptiste Jadot,¹ Jing Li,³ Pierre-André Mortemousque,² Louis Hutin,² Romain Maurand,³ Xavier Jehl,³ Marc Sanquer,³ Silvano De Franceschi,³ Christopher Bäuerle,¹ Franck Balestro,¹ Yann-Michel Niquet,³ Maud Vinet,² Tristan Meunier,¹ and Matias Urdampilleta^{1,†}

¹Université Grenoble Alpes, CNRS, Grenoble INP, Institut Néel, 38402 Grenoble, France

²CEA, LETI, Minatèc Campus, 38054 Grenoble, France

³Université Grenoble Alpes, CEA, IRIG, 38000 Grenoble, France

(Received 26 January 2020; revised 27 May 2020; accepted 16 June 2020; published 24 August 2020)

The recent development of arrays of quantum dots in semiconductor nanostructures highlights the progress of quantum devices toward a large scale. However, how to realize such arrays on a scalable platform such as silicon is still an open question. One of the main challenges lies in the detection of charges within the array. It is a prerequisite to initialize a desired charge state and read out spins through spin-to-charge conversion mechanisms. In this work, we use two methods based on either a single-lead charge detector or a reprogrammable single-electron transistor. By these methods, we study the charge dynamics and sensitivity by performing single-shot detection of the charge. Finally, we can probe the charge stability at any node of a linear array and assess the Coulomb disorder in the structure. We find an electrochemical potential fluctuation induced by charge noise comparable to that reported in other silicon quantum dots.

DOI: 10.1103/PhysRevApplied.14.024066

I. INTRODUCTION

The ability to create long-lifetime qubits out of single electron spins in lithographically defined quantum dots (QDs) has turned silicon into a promising platform for quantum computing. The long coherence time of spins embedded in isotopically enriched silicon combined with improved control of coherent manipulations allows high-fidelity single-qubit and two-qubit gates [1–4]. Moreover, recent developments have shown that spin readout can be performed with high fidelity and on a short timescale [5–8], making error-correction codes possible in scalable architectures [9–11]. Following this progress, the next milestone is to increase the number of qubits under control while preserving the performances mentioned above.

In addition, two-dimensional arrays of quantum dots have recently been explored [12], in which basic quantum functionalities [13] as well as condensed-matter simulations [14] have been demonstrated. However, these

demonstrations were achieved in GaAs heterostructures where the hyperfine interaction limits the coherence time to a few tens of nanoseconds. To create functional quantum-dot arrays on a more-scalable platform, such as silicon quantum dots [15–18], the same level of control and addressability needs to be achieved.

In this paper, we report a first important step toward this goal. In an architecture that contains eight MOS quantum dots, see Fig. 1, we demonstrate how to perform remote charge sensing of the different single QDs and double QDs (DQDs) using embedded detectors. Each QD is operated with a single gate electrode: the experiment is conducted on a four-split-gate *n*-type silicon device, fabricated on a silicon-on-insulator 300-mm wafer using an industry-standard fabrication line. We propose two detection schemes based on a charge sensor embedded in the device that allows us to probe the charge stability and dynamics in the different QD configurations as well as the Coulomb disorder in the structure. Moreover, these detection methods allow us to assess the static and dynamical Coulomb disorder, which is an important characterization step to understand and increase the quality of qubit devices.

The first charge-detection method consists in using a single-lead quantum dot (SLQD) at one end of the array, probed by radio-frequency (rf) reflectometry [19]. This method has very high charge sensitivity to the first and

*emmanuel.chanrion@neel.cnrs.fr

†matias.urdampilleta@neel.cnrs.fr

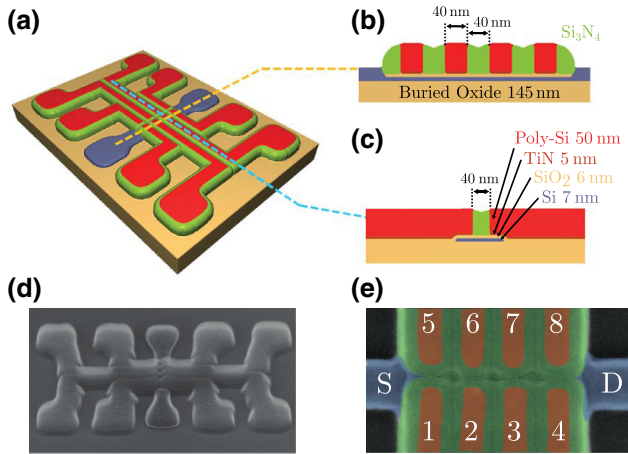


FIG. 1. (a) The 2×4 QD array. The silicon nanowire (blue) is covered with top gates (red), which are separated by spacers (green). The noncovered regions of the nanowire are highly doped to form electron reservoirs. (b) Cross section along the nanowire. (c) Cross section along one top gate. (d) SEM micrograph of a device similar to the ones used in the present study. (e) False-color SEM micrograph of the array using the same color code as in (a). The quantum dots (QD1–QD8) are localized below the top gates (1–8) in the corners of the nanowire. D, drain; S, source.

second neighbors as well as high single-shot charge-readout fidelity (99.9% at 1 kHz). Moreover, this approach is less demanding in terms of its footprint, compared with use of a standard rf single-electron transistor (SET), as it requires only one gate and one reservoir to achieve the readout. We can envision using this SLQD as a readout site in quantum protocols using spin shuttling at one end of the array for qubit readout [20,21] or in three-dimensional structures [22,23]. The second method relies on a reconfigurable SET [17]. For this purpose, one can use any of the QDs of the upper or lower linear array. It allows us to sense any quantum dot in the other parallel array and shows, as well, high single-shot charge fidelity.

The paper is organized as follows. We first describe how the devices are designed and operated. Secondly, we discuss how the SLQD- and SET-based detectors work and how we operate them to probe the stability diagrams of the neighboring double quantum dots in the few-electron regime. Then, we use these two methods to investigate single-shot detection of charge tunneling in the array and the Coulomb disorder inside the device. Finally, we conclude by discussing how these two sensing methods could be used in a protocol to form a logical qubit in a one-dimensional (1D) array of quantum dots [24].

II. DEVICE DESIGN AND OPERATION

The devices, such as the one depicted in Fig. 1, are fabricated on 300-mm silicon-on-insulator substrates (buried

oxide thickness 145 nm), see Fig. 1(b). The silicon channel (width 70 to 110 nm) is defined by mesa patterning. The gate stack [see Fig. 1(c)] is made of 6-nm thermally grown SiO_2 , 5-nm atomic layer deposition-deposited TiN, and 50-nm poly-Si, topped with a bilayer hard mask with 30-nm SiN and 25-nm SiO_2 . A hybrid deep-UV–electron-beam gate-patterning scheme is implemented, in which multiple lithography-etch cycles are performed sequentially to transfer parts of the final pattern into the hard mask, before a final transfer etch. The resulting structure consists of four pairs of split gates along a silicon-nanowire channel, each overlapping opposite edges of the mesa. The gate pitch along the nanowire direction is 80 nm (gate with length 40 nm, spaced by 40 nm), and the split width is 40 nm. The doped areas are defined in a self-aligned way: the regions covered by the gates and an offset spacer act as a mask for dopant implantation. Thus, a particularly wide (35-nm) Si_3N_4 offset spacer is deposited, completely covering the intergate spacings. The Si areas still exposed are regrown by means of epitaxy, before undergoing ion implantation of *n*-type dopants activated by a N_2 spike anneal. These regions form the electron reservoirs, labeled “S” and “D” (for “source” and “drain”) in the figures by analogy with classic MOS devices.

Once the device cools down to dilution-fridge temperature ($T_{\text{base}} = 40$ mK, $T_e = 150$ mK), quantum dots can form at the Si/SiO_2 interface by application of a positive voltage on the top gates, as previously reported. This allows us to form up to 2×4 quantum dots, one dot underneath each gate electrode; see Fig. 1(e).

To sense single charges in the nanostructure, we use two different methods. The first one consists in using a SLQD as a charge detector. It is positioned next to a reservoir at the left end of the gate array and is probed by radio-frequency gate reflectometry. For this purpose, the gate controlling its electrochemical potential is connected to a tank circuit formed by an inductance and the parasitic capacitance to ground. Therefore, the phase of the reflected signal is sensitive to a change in quantum capacitance. The phase shift exhibits a Coulomb-like peak when a level of the SLQD is in resonance with the Fermi sea of the lead. To sense the charge occupancy of neighboring dots, the SLQD is biased on the side of such a peak. In this position, no current flows through the device due to large negative voltages applied to the gates next to the drain (gates 3, 4, 7, and 8), efficiently closing the barrier to that reservoir. Any change in the electrostatic environment induces a shift of the Coulomb peak and thereby alters the reflected rf signal. As described in the next section, this method allows us to sense the first and second neighbors of the SLQD.

The second charge-sensing method consists in operating the upper side of the 2×4 array as a SET. For this purpose, three of the four upper gates are set to 1.2 V, which corresponds to a regime where these quantum dots act as electron reservoirs. The last gate controls the SET,

which is operated in the many-electron regime. Similarly to the previous method, the embedded SET is biased on a Coulomb peak to reach maximum sensitivity. It is worth noting that to minimize tunneling effects between the SET and the probed quantum dot, we implement this method in a wide wire device (110 nm).

III. CHARGE DETECTION IN THE ARRAY

A. Charge sensing using a rf single-lead quantum dot

To demonstrate charge sensing by dispersive readout, we first focus on the 2×2 subarray depicted in Fig. 2(a). It consists of one QD used as an electrometer and three QDs that are probed. The other gates are set to -1 V to decouple the array from the drain reservoir. In this configuration, we use QD5 as an electrometer and relabel it as “SLQD” to distinguish it from the probed QDs (QD1, QD2, and QD6). We connect the gate controlling the SLQD to an inductance $L = 820$ nH to achieve dispersive sensing of the electrometer, as depicted in Fig. 2(b). Together with the parasitic capacitance to ground $C_p = 0.39$ pF, we obtain an LC circuit with resonant frequency $f = 286$ MHz and quality factor $Q = 70$. The signal once demodulated gives the amplitude and phase shift of the reflected radio-frequency wave. The maximum phase shift is measured on the top of a Coulomb peak and is directly related to the quantum capacitance, C_Q , $\Delta\Phi \simeq 2Q \times C_Q/C_p$ [25]. We obtain $\Delta\Phi = 1$ mrad and $C_Q = 3$ aF on average for the peak shown in Fig. 2(c).

Figure 2(c) shows such a Coulomb peak as a function of the gate voltage controlling QD1. The slope of the detector against V_1 is due to capacitive coupling between the SLQD and gate 1. The addition of one charge in QD1 induces an abrupt voltage shift ΔV of the position of the electrometer Coulomb peak. Figure 2(d) shows the extended charge-stability diagram, where the filling of QD1 with up to six electrons is observed.

The shift of the SLQD chemical potential induced by charging events is larger than the Coulomb-peak linewidth. Since the detector sensitivity vanishes outside this peak, feedback loop-assisted detection is impractical in this case. Nevertheless, we can bias the SLQD at a fixed voltage in order to sense one charge being exchanged between the lead and a dot or between two dots in the DQD configuration formed by (QD1, QD2) and (QD2, QD6). Figures 3(a) and 3(b) show the stability diagram of the two DQDs in the few-electron regime. It is important to note that the shift induced by a charge in QD6 (4.7 linewidths) is stronger than that induced in QD2 or QD1 (1.1 and 2.4 linewidths, respectively). This can be explained by the localization of the quantum dot in the corner of the nanowire [26]. Therefore, the capacitive and tunnel coupling along the nanowire axis is stronger than along the transverse axis.

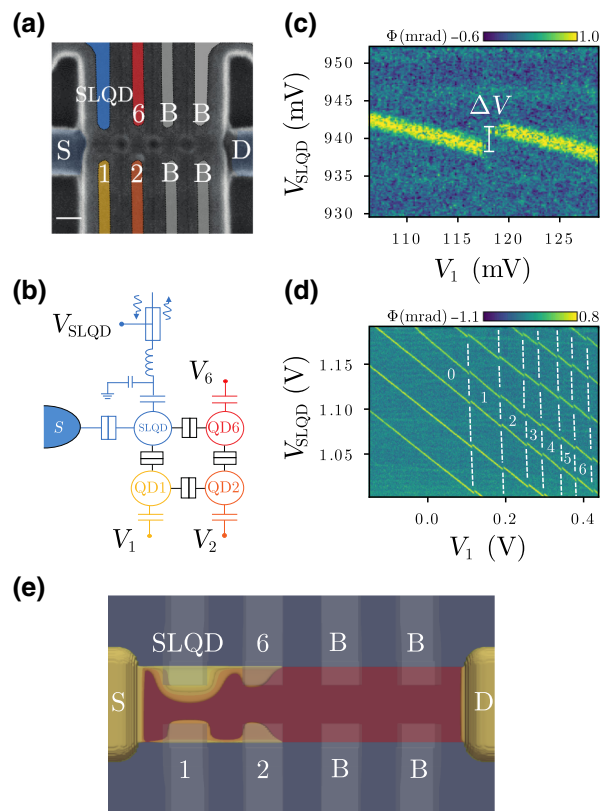


FIG. 2. (a) False-color SEM micrograph of the QD configuration in the SLQD detection mode. “B” stands for “barrier gates,” where the voltage is set to -1 V. (b) Equivalent electrical circuit of the device probed by dispersive readout. One quantum dot is used as an electrometer (SLQD) and is tunnel and capacitively coupled to the three neighboring QDs. Its gate is connected to an inductance to form an LC resonant circuit that is probed by rf reflectometry. (c) Phase change of the resonant circuit as a function of V_{SLQD} and V_1 . The signal lines correspond to a charge degeneracy of the electrometer dot, which experiences a shift in voltage for one electron added to QD1. The voltage shift corresponds to 2.4 linewidths of the detector. (d) Charge-stability diagram for QD1. (e) Simulation of the electron density inside the channel under the same polarization conditions as in the experiment and using the Thomas-Fermi approximation. A large density of electrons is present at the SLQD location, which overlaps with the QD6 potential. A large dot accumulates under the SLQD gate, and tends to spill over QD6, to which it is strongly coupled. D, drain; S, source.

To confirm this hypothesis, we compute the carrier density in a self-consistent Thomas-Fermi approximation. The source and drain are assumed to be doped with phosphorous ($N_d = 10^{20}/\text{cm}^3$), whose ionization probabilities are calculated with an incomplete ionization model that is valid at low temperature [27]. The density of electrons, $n(\mathbf{r}) = N_c F_{1/2} \{[E_c - eV(\mathbf{r}) - \mu]/kT\}$, depends on the local potential $V(\mathbf{r})$, which includes the mean-field contribution from the ionized impurities and electrons

themselves ($F_{1/2}$ being the Fermi integral, N_c the effective density of states, E_c the conduction-band edge energy in bulk silicon, and μ the chemical potential). The self-consistent calculations are performed at $T = 20$ K [the charge density being converged on the scale of Figs. 2(e) and 4(e) but the convergence being increasingly difficult at lower temperatures]. Although the Thomas-Fermi approximation does not account for quantum effects such as confinement and tunneling, it gives a fair account of the position of the dots and transport channels in the system. Figure 2(e) shows that a large dot forms under the SLQD gate, as expected. It tends to spill under the neighboring QD6 gate, while it remains fairly decoupled from the facing QD1 and QD2, which is in good qualitative agreement with the experiments. It is also worth noting that, in this configuration, the QDs are not evenly coupled to the reservoirs. QD1 is strongly coupled to the reservoir, while QD2 is only weakly coupled. QD6 is only weakly coupled to the source but can exchange an electron directly with the SLQD, which is always resonant with the reservoir Fermi sea during measurement.

The sensitivity of the detector is limited from one to a few charge transitions before the signal vanishes. A working sensing position can be held only for voltage offsets $\Delta V_1, \Delta V_2 \sim 20$ mV, due to the small detector linewidth and strong capacitive coupling. However, the coarse tuning of a double quantum dot such as (QD1, QD2) implies exploring a voltage space (V_1, V_2) that can be as large as 1×1 V². To facilitate this tuning despite the absence of a feedback loop, we calibrate the SLQD detector over the whole voltage space. For this purpose, we measure the shift in SLQD chemical potential at the boundaries of this voltage space and we interpolate the optimum window for the detector for each point assuming a constant-capacitive-coupling model. This method makes the sensor sensitive over the whole region probed, as illustrated in Fig. 3(c), which shows the stability diagram of the (QD2, QD6) DQD over many charge configurations. It is also possible to probe extended QD combinations as illustrated in Supplemental Material A [28], where triple-dot charge stabilities are explored.

B. Charge sensing using an embedded SET

To probe the charge and spin configuration of QDs located deeper in the array, the above solution requires shuttling electrons to one of the neighboring dots, as the SLQD is not sensitive to QD3, QD4, QD7, and QD8. However, such a protocol requires fine control of tunnel barriers on fast timescales. Another approach we use here is to operate the upper part of the array as a reconfigurable SET. For this purpose, all the gates but one are set to accumulation mode (greater than 1.2 V) to extend the reservoirs as close as possible to the SET [see Fig. 4(a)]. We check that we can form a SET with the last gate left

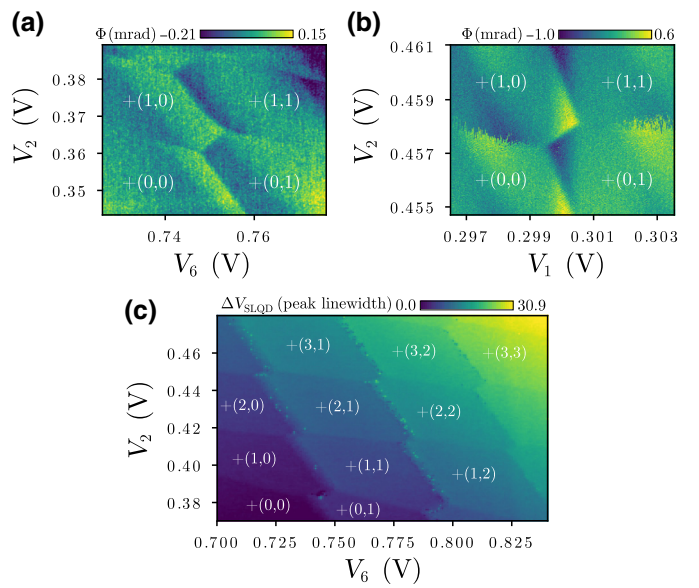


FIG. 3. (a),(b) Stability diagrams for the (QD2, QD6) and (QD1, QD2) DQDs. The dispersive signal from the SLQD is plotted as a function of (V_2, V_6) and (V_1, V_2) . (c) Stability diagram for the (QD2, QD6) DQD for extended charge configurations. We plot the shift in detector position (normalized by the peak linewidth) induced by a change in charge occupancy as a function of V_2 and V_6 . For each plot, the charge labeling is relative to the state at the bottom left of the diagram.

by measuring a Coulomb map that exhibits a regular pattern of Coulomb diamonds (see Supplemental Material B [28]). Figure 4(b) presents the stability diagram for the SLQD and QD2 probed with this technique. Similarly to the SLQD method, one can clearly see a shift in voltage on the detector for every electron accumulated in QD2.

To sense a multi-QD system such as the (QD2, QD3) DQD, the formation of a single SET localized under one gate is not very efficient. The presence of the SET reservoir screens the capacitive coupling to other QDs across the wire, which limits the sensitivity of the SET to a single QD. This is supported qualitatively by the simulation presented in Fig. 4(e). It shows that the accumulation of electrons under one of the reservoir gate expands inside the channel toward one of the facing QDs. Therefore, we use another strategy, which consists in forming SETs in series along the nanowire axis; see Fig. 4(c). They are operated in the tunnel-broadened and large-bias (greater than 3 mV) regime in order to lift Coulomb blockade and have a finite current flowing through the SETs at any voltage. Figure 4(d) shows the (QD2, QD3) DQD stability diagram in the few-electron regime probed by two serial SETs. However, we operate the double SET in a regime where Coulomb oscillations are less sharp than in the case of a single SET, which decreases the sensitivity.

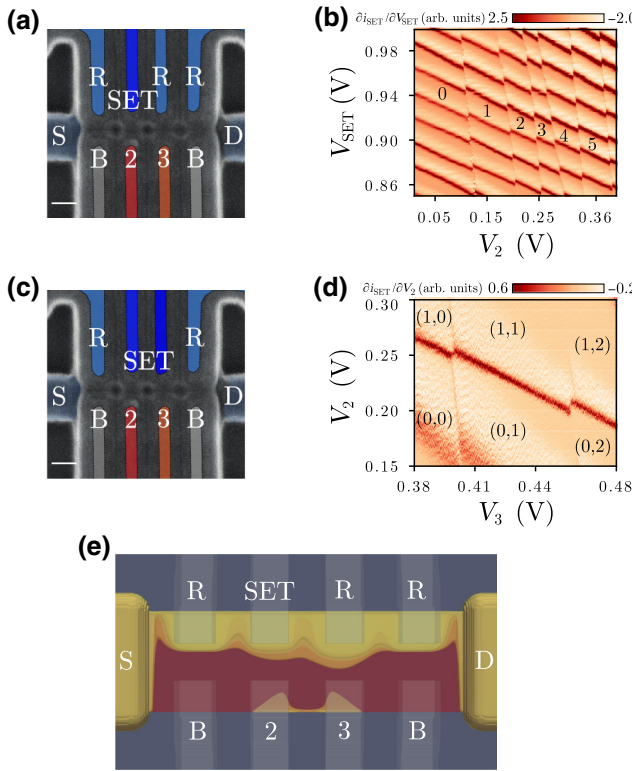


FIG. 4. (a) False-color SEM micrograph of the QD configuration in the SET detection mode. “B” stands for “barrier” ($V = -1$ V) and “R” stands for “reservoir” ($V = 1.2$ V). (b) Charge-stability diagram for QD2. The derivative of the current through the device is plotted as a function of V_{SET} and V_2 . In this case, the QD in front of QD2 is operated as a SET, while the other upper gates are set to high positive voltages (greater than 1.2 V) to extend the reservoirs close to the SET. (c) False-color SEM micrograph of the QD configuration in the double-SET detection mode. The top linear array of quantum dots is operated as two SETs in series. The Coulomb blockade is probed by our measuring the current flowing through the structure. (d) Stability diagram for a (QD2, QD3) DQD in the few-electron regime. The detector is operated in the large-bias regime (3 mV) to extend the region of sensitivity without the need for capacitive compensation. (e) Isodensity surfaces inside the channel computed in the Thomas-Fermi approximation at the following gate biases: $V = -1$ V on the barrier gates, $V = 1.2$ V on the reservoir gates, $V = 0.8$ V on the SET, and $V = 0.3$ V on QD2 and QD3. As the bias is larger on the reservoir gates than on the SET, and because of the cross-capacitance between the upper and lower gates, the density in the SET reservoirs tends to spill toward QD3. This will further decrease the sensitivity of the SET to changes in the occupation of QD3. D, drain; S, source.

IV. PROBING SINGLE CHARGE TUNNELING AND COULOMB DISORDER

A. Time-resolved charge detection

The readout of spin qubits in semiconductor quantum dots is achieved by mapping the spin information on the

charge degree of freedom through energy-selective tunneling [35], tunnel rate-selective tunneling [36], or Pauli spin blockade between two QDs [37,38]. Hence, the ability to perform high-fidelity single-shot readout of a single charge tunneling is a key requirement for quantum computation using spin qubits. Here we demonstrate the single-shot readout of charge using the two detection methods described earlier.

To isolate a charge-tunneling event in the measurement bandwidth (1 kHz), we focus on QD2, which is only slightly coupled to the reservoir when V_1 is set to 0 V. The slow tunneling of the charge, already evidenced by the noncontinuous delineation between charge configuration (0,0) and charge configuration (1,0), for instance [see Fig. 3(b)], is measured as a function of time with the two different detection methods; see Figs. 5(a) and 5(c). In these two graphs, we can observe the charge tunneling in QD2 while the detector experiences a shift in phase or in current.

To analyze the signal-to-noise ratio, we first load an electron on QD2 and then pulse the QD2 chemical potential above the Fermi sea. Using this method, we perform 8000 single-shot measurements at a time where there is equal probability to have QD2 loaded or empty. We integrate the signal for 1 nm and plot the resulting phase shift as a histogram; see Figs. 5(b) and 5(d). The data are fitted with two Gaussian curves to extract the theoretical error in discriminating between the two charge states. The minimal error rate on a charge assignment is 10^{-3}

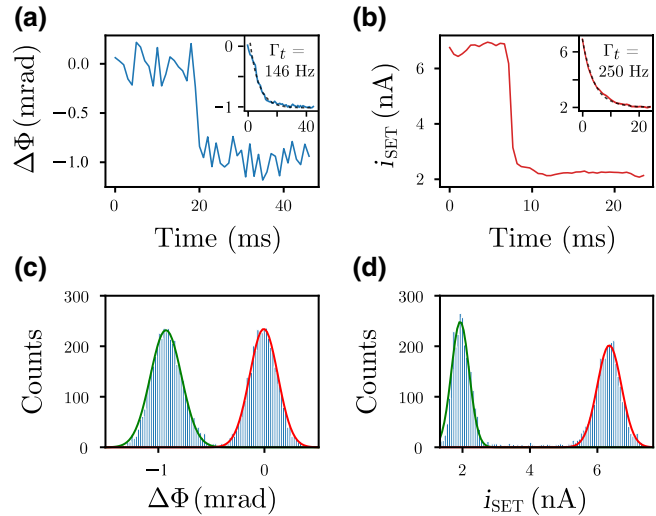


FIG. 5. Time-resolved measurement of a single charge tunneling out of QD2 probed by (a) dispersive and (b) current-based measurement for an integration time of 1 ms. The insets show the average of 150 time traces (solid lines). The QD2-lead tunnel rate Γ_t is extracted with use of an exponential-decay model (dashed black line). (c),(d) Histograms of 8000 single-shot measurements with an integration of 1 ms. The signal-to-noise ratios are 7 and 15, respectively.

for the SLQD-based readout and 10^{-7} for the embedded single-SET-based readout. Moreover, the signal-to-noise ratio gives a time-domain charge sensitivity of 5.0×10^{-3} and $2.1 \times 10^{-3} e/\sqrt{\text{Hz}}$, respectively. These values are comparable to what has been reported in the literature [15,39] but could be increased. In the case of dispersive readout and large tunnel coupling compared with temperature, the maximum phase shift is given by $\Delta\Phi_{\max} = 2Q \times (e\alpha)^2 / \pi t C_p$, with α the lever arm and t the tunnel coupling between the lead and the SLQD [40]. Hence, the signal could be increased by controlling the tunnel coupling using an extra gate or by increasing the capacitive coupling between the SLQD and its top gate. The noise on our measurement is estimated to be around $0.1 \text{ nV}/\sqrt{\text{Hz}}$, which is equivalent to a noise temperature of 4.5 K and corresponds to the noise of the cryogenic amplifier used here. Noise could be reduced by use of a superconducting amplifier such as a Josephson parametric amplifier [41], which would decrease the noise temperature by more than 1 order of magnitude. In the case of the embedded-SET-based measurement, the amplitude of the signal can be increased by use of modern transimpedance amplifiers, which are now operational at dilution temperatures [42].

B. Low-frequency charge noise and static Coulomb disorder

The two methods we develop enable measurement of the charge dynamics of single-electron tunneling in quantum dots but can also be used to probe the charge noise within the structure. Charge noise may be the ultimate source of decoherence in isotopically purified silicon, due to finite spin-orbit coupling or the presence of an inhomogeneous magnetic field [3]. It is therefore crucial to understand its origin to increase the single-qubit-gate and two-qubit-gate fidelities.

In this context, we operate the top array as a single SET to assess the charge noise inside the structure. We then measure the noise spectrum on the chemical potential induced by charge fluctuations, S_μ , at two different points of the SET Coulomb peak, depicted in Fig. 6(a). At these points the slope is maximum, giving access to the highest charge sensitivity. Figure 6(b) presents the two corresponding charge-noise spectra. The first spectrum shows a $1/f^\beta$ behavior, with $\beta = 1.14$, which is close to the $1/f$ behavior expected for a uniform distribution of fluctuating two-level systems (TLSs) in the environment [29]. It is worth noting that the chemical potential fluctuation at 1 Hz is lower than $1 \mu\text{eV}/\sqrt{\text{Hz}}$, which compares favorably with the lowest potential-fluctuation values reported in the literature for silicon, which are in the $2\text{--}5 \mu\text{eV}/\sqrt{\text{Hz}}$ range at 350 mK [30–32,34]. The second spectrum shows a stronger deviation from $1/f$ noise. To explain this, we use a more-refined model of charge noise that accounts for

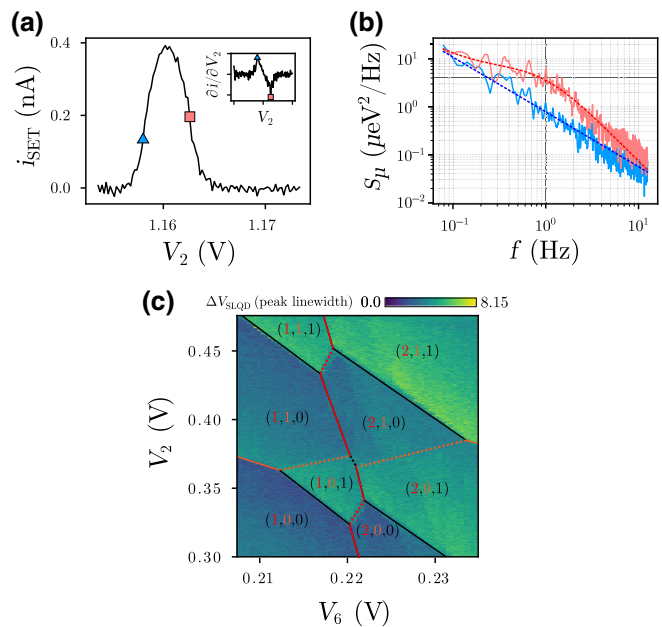


FIG. 6. (a) Coulomb peak of the SET located under V_2 . The inset shows derivative of the current against the gate voltage. (b) Power spectral density of the noise in the chemical potential on the two sides of the Coulomb peak at 350 mK . The blue curve is fit with use of a $1/f^\beta$ model ($\beta = 1.14$) and the red curve is fit with a function of the form $A/f^\beta + B/f^2/f_c^2 + 1$ ($\beta = 1.4$ and $f_c = 1 \text{ Hz}$). (c) Stability diagram for the triple-dot system formed by QD2, QD6, and a defect in the channel.

a nonuniform distribution of TLS activation energies compared with the temperature [30,33]. S_μ is fit with a function of the form $S_\mu = A/f^\beta + B/f^2/f_c^2 + 1$. The Lorentzian shape visible in Fig. 6(b) suggests the presence of a single fluctuator whose characteristic frequency, f_c , is centered at 1 Hz. However, the amplitude of the potential fluctuation at 1 Hz is around $2 \mu\text{eV}/\sqrt{\text{Hz}}$, which indicates that the TLS is only slightly coupled to the quantum dot. The discrepancy between the two probed spectra for the two different V_2 values can be explained by a full depletion of the charge trap at lower gate voltage. However, further investigations are required to understand the nature of the trap and its location.

While mobile charges can affect spin-qubit coherence, fixed charges can be detrimental for the production of QDs with low dot-to-dot variability. Indeed, the presence of static disorder modifies the electrostatic environment of the QD. We can probe the formation of unintentional quantum dots by charge sensing. Figure 6(c) shows an example of a stability diagram measured between QD2 and QD6. The presence of an accidental quantum dot is clearly visible as the expected honeycomb pattern is not visible. Instead, we obtain different charge configurations when QD2 and QD6 exchange an electron with the defect. These kinds of signatures are visible in a few of the stability diagrams

(see Supplemental Material A [28]) and can be attributed to unintentional doping of the channel during the formation of the source and drain. To avoid the presence of these fixed charges in the channel, other fabrication routes are currently under investigation. For instance, the epitaxial formation of reservoirs is an alternative to dopant implantation as it will reduce the amount of unintentional dopants in the channel due to high-energy implantation.

V. CONCLUSION

In conclusion, we show the ability to build a device with a large number of quantum dots capacitively and tunnel coupled. The charge occupancy of any of the quantum dots in the structure can be probed using either a reconfigurable SET or a SLQD. Moreover, we demonstrate that these two methods offer the ability to perform real-time measurement of a single charge-tunneling event, which could be used to load single electrons in the structure or read out spin states. Finally, we use these methods to assess the static and dynamical Coulomb disorder in the structure.

We propose operating a $2 \times N$ array of QDs to form a 1D array of $N - 2$ qubits using the detection methods presented to initialize, displace and read out the qubits. First, initialization is performed with the lower 1D array used as a reconfigurable SET to monitor the loading and motion of single charges in the upper array. Then, SLQDs that are located at both ends of the top row are used to perform readout on the adjacent dot in the same row. For this purpose, we perform spin-to-charge conversions based on Pauli-spin blockade between the qubit and the SLQD [7]. Finally, the other single-electron qubits are read out similarly after being shuttled next to the SLQD. Such operations require good control of the array charge occupancy and fine control of tunnel barriers [13,18].

ACKNOWLEDGMENTS

We acknowledge technical support from P. Perrier, H. Rodenas, E. Eyraud, D. Lepoittevin, I. Pheng, T. Crozes, L. Del Rey, D. Dufeu, J. Jarreau, J. Minet, and C. Guttin. E.C. acknowledges support from the Agence Nationale de la Recherche (Grant No. ANR-15-IDEX-02). D.J.N. and C.S. acknowledge the GreQuE doctoral programs (Grant Agreement No. 754303). The device fabrication is funded through the Mosquito project (Grant Agreement No. 688539) and QuCube (Grant Agreement No. 810504). This work is supported by the Agence Nationale de la Recherche through the MAQSi, CMOSQSPIN, and CODAQ projects (Grant No. ANR-16-ACHN-0029).

[1] D. M. Zajac, A. J. Sigillito, M. Russ, F. Borjans, J. M. Taylor, G. Burkard, and J. R. Petta, Resonantly driven cnot gate for electron spins, *Science* **359**, 439 (2018).

- [2] T. F. Watson, S. G. J. Philips, E. Kawakami, D. R. Ward, P. Scarlino, M. Veldhorst, D. E. Savage, M. G. Lagally, M. Friesen, S. N. Coppersmith, M. A. Erikson, and L. M. K. Vandersypen, A programmable two-qubit quantum processor in silicon, *Nature* **555**, 633 (2018).
- [3] J. Yoneda, K. Takeda, T. Otsuka, T. Nakajima, M. Delbecq, G. Allison, T. Honda, T. Kodera, S. Oda, Y. Hoshi, *et al.*, A quantum-dot spin qubit with coherence limited by charge noise and fidelity higher than 99.9%, *Nat. Nanotech.* **13**, 102 (2018).
- [4] W. Huang, C. H. Yang, K. W. Chan, T. Tanttu, B. Hensen, R. C. C. Leon, M. A. Fogarty, J. C. C. Hwang, F. E. Hudson, K. M. Itoh, A. Morello, A. Laucht, and A. S. Dzurak, Fidelity benchmarks for two-qubit gates in silicon, *Nature* **569**, 532 (2019).
- [5] G. Zheng, N. Samkharadze, M. L. Noordam, N. Kalhor, D. Brousse, A. Sammak, G. Scappucci, and L. M. K. Vandersypen, Rapid gate-based spin read-out in silicon using an on-chip resonator, *Nat. Nanotechnol.* **14**, 742 (2019).
- [6] D. Keith, M. G. House, M. B. Donnelly, T. F. Watson, B. Weber, and M. Y. Simmons, Single-Shot Spin Readout in Semiconductors Near the Shot-Noise Sensitivity Limit, *Phys. Rev. X* **9**, 041003 (2019).
- [7] M. Urdampilleta, D. J. Niegemann, E. Chanrion, B. Jadot, C. Spence, P.-A. Mortemousque, C. Bäuerle, L. Hutin, B. Bertrand, S. Barraud, R. Maurand, M. Sanquer, X. Jehl, S. De Franceschi, M. Vinet, and T. Meunier, Gate-based high fidelity spin readout in a CMOS device, *Nat. Nanotechnol.* **14**, 737 (2019).
- [8] A. West, B. Hensen, A. Jouan, T. Tanttu, C. H. Yang, A. Rossi, M. F. Gonzalez-Zalba, F. E. Hudson, A. Morello, D. J. Reilly, and A. S. Dzurak, Gate-based single-shot readout of spins in silicon, *Nat. Nanotechnol.* **14**, 437 (2019).
- [9] R. Li, L. Petit, D. P. Franke, J. P. Dehollain, J. Helsen, M. Steudtner, N. K. Thomas, Z. R. Yoscovits, K. J. Singh, S. Wehner, *et al.*, A crossbar network for silicon quantum dot qubits, *Sci. Adv.* **4**, eaar3960 (2018).
- [10] M. Veldhorst, H. G. J. Eenink, C. H. Yang, and A. S. Dzurak, Silicon cmos architecture for a spin-based quantum computer, *Nat. Commun.* **8**, 1766 (2017).
- [11] L. Hutin, S. De Franceschi, T. Meunier, and M. Vinet, Quantum device with spin qubits. US Patent App. 15/967, 778 (2018).
- [12] U. Mukhopadhyay, J. P. Dehollain, C. Reichl, W. Wegscheider, and L. M. K. Vandersypen, A 2×2 quantum dot array with controllable inter-dot tunnel couplings, *Appl. Phys. Lett.* **112**, 183505 (2018).
- [13] P. A. Mortemousque, E. Chanrion, B. Jadot, H. Flentje, A. Ludwig, A. D. Wieck, M. Urdampilleta, C. Bauerle, and T. Meunier, arXiv:1808.06180 (2018).
- [14] J. P. Dehollain, U. Mukhopadhyay, V. P. Michal, Y. Wang, B. Wunsch, C. Reichl, W. Wegscheider, M. S. Rudner, E. Demler, and L. M. K. Vandersypen, Nagaoka ferromagnetism observed in a quantum dot plaquette, *Nature* **579**, 528 (2020).
- [15] D. M. Zajac, T. M. Hazard, X. Mi, E. Nielsen, and J. R. Petta, Scalable Gate Architecture for a One-Dimensional Array of Semiconductor Spin Qubits, *Phys. Rev. Appl.* **6**, 054013 (2016).

- [16] A. C. Betz, M. L. V. Tagliaferri, M. Vinet, M. Broström, M. Sanquer, A. J. Ferguson, and M. F. Gonzalez-Zalba, Reconfigurable quadruple quantum dots in a silicon nanowire transistor, *Appl. Phys. Lett.* **108**, 203108 (2016).
- [17] W. I. L. Lawrie, H. G. J. Eenink, N. W. Hendrickx, J. M. Boter, L. Petit, S. V. Amitonov, M. Lodari, B. Paquelet Wuetz, C. Volk, S. G. J. Philips, G. Droulers, N. Kalhor, F. van Riggelen, D. Brousse, A. Sammak, L. M. K. Vandersypen, G. Scappucci, and M. Veldhorst, Quantum dot arrays in silicon and germanium, *Appl. Phys. Lett.* **116**, 080501 (2020).
- [18] F. Ansaloni, A. Chatterjee, H. Bohuslavskyi, B. Bertrand, L. Hutin, M. Vinet, and F. Kuemmeth, Single-electron control in a foundry-fabricated two-dimensional qubit array, arXiv:2004.00894 (2020).
- [19] M. G. House, I. Bartlett, P. Pakkiam, M. Koch, E. Peretz, J. van der Heijden, T. Kobayashi, S. Rogge, and M. Y. Simmons, High-Sensitivity Charge Detection with a Single-Lead Quantum dot for Scalable Quantum Computation, *Phys. Rev. Appl.* **6**, 044016 (2016).
- [20] T. Fujita, T. A. Baart, C. Reichl, W. Wegscheider, and L. M. K. Vandersypen, Coherent shuttle of electron-spin states, *npj Quantum Inf.* **3**, 22 (2017).
- [21] A. R. Mills, D. M. Zajac, M. J. Gullans, F. J. Schupp, T. M. Hazard, and J. R. Petta, Shuttling a single charge across a one-dimensional array of silicon quantum dots, *Nat. Commun.* **10**, 1063 (2019).
- [22] P. Batude, L. Brunet, C. Fenouillet-Beranger, F. Andrieu, J. Colinge, D. Lattard, E. Vianello, S. Thuries, O. Billoint, P. Vivet, *et al.*, in *IEEE International Electron Devices Meeting* (IEEE, San Francisco, CA, USA, 2017).
- [23] G. Larrieu and X.-L. Han, Vertical nanowire array-based field effect transistors for ultimate scaling, *Nanoscale* **5**, 2437 (2013).
- [24] C. Jones, M. A. Fogarty, A. Morello, M. F. Gyure, A. S. Dzurak, and T. D. Ladd, Logical Qubit in a Linear Array of Semiconductor Quantum Dots, *Phys. Rev. X* **8**, 021058 (2018).
- [25] M. Jung, M. D. Schroer, K. D. Petersson, and J. R. Petta, Radio frequency charge sensing in InAs nanowire double quantum dots, *Appl. Phys. Lett.* **100**, 253508 (2012).
- [26] B. Voisin, V.-H. Nguyen, J. Renard, X. Jehl, S. Barraud, F. Triozon, M. Vinet, I. Duchemin, Y.-M. Niquet, S. De Franceschi, and M. Sanquer, Few-electron edge-state quantum dots in a silicon nanowire field-effect transistor, *Nano Lett.* **14**, 2094 (2014).
- [27] P. P. Altermatt, A simulation model for the density of states and for incomplete ionization in crystalline silicon. II. Investigation of Si:As and Si:B and usage in device simulation, *J. Appl. Phys.* **100**, 113715 (2006).
- [28] See Supplemental Material at <http://link.aps.org/supplemental/10.1103/PhysRevApplied.14.024066> for a demonstration of a triple quantum dots in the few-electron regime using SLQD- and SET-based sensing, a Coulomb map of a single-QD SET, and stability diagrams for QDs in the lower array probed by a reconfigurable SET.
- [29] E. Paladino, Y. M. Galperin, G. Falci, and B. L. Altshuler, 1/f noise: Implications for solid-state quantum information, *Rev. Mod. Phys.* **86**, 361 (2014).
- [30] E. Connors, J. J. Nelson, H. Qiao, L. F. Edge, and J. M. Nichol, Low-frequency charge noise in Si/SiGe quantum dots, *Phys. Rev. B* **100**, 165305 (2019).
- [31] B. Freeman, J. Schoenfield, and H. Jiang, Comparison of low frequency charge noise in identically patterned Si/SiO₂ and Si/SiGe quantum dots, *Appl. Phys. Lett.* **108**, 253108 (2017).
- [32] J.-S. Kim, T. M. Hazard, A. A. Houck, and S. A. Lyon, A low-disorder metal-oxide-silicon double quantum dot, *Appl. Phys. Lett.* **114**, 043501 (2019).
- [33] P. Dutta, P. Dimon, and P. M. Horn, Energy Scales for Noise Processes in Metals, *Phys. Rev. Lett.* **43**, 646 (1979).
- [34] X. Mi, S. Kohler, and J. Petta, Landau-Zener interferometry of valley-orbit states in Si/SiGe double quantum dots, *Phys. Rev. B* **98**, 161404 (2018).
- [35] J. M. Elzerman, R. Hanson, L. H. Willems van Beveren, B. Witkamp, L. M. K. Vandersypen, and L. P. Kouwenhoven, Single-shot read-out of an individual electron spin in a quantum dot, *Nature* **430**, 431 (2004).
- [36] R. Hanson, L. H. Willems van Beveren, I. T. Vink, J. M. Elzerman, W. J. M. Naber, F. H. L. Koppens, L. P. Kouwenhoven, and L. M. K. Vandersypen, Single-Shot Readout of Electron Spin States in a Quantum dot Using Spin-Dependent Tunnel Rates, *Phys. Rev. Lett.* **94**, 196802 (2005).
- [37] K. Ono, D. G. Austing, Y. Tokura, and S. Tarucha, Current rectification by pauli exclusion in a weakly coupled double quantum dot system, *Science* **297**, 1313 (2002).
- [38] C. Barthel, D. J. Reilly, C. M. Marcus, M. P. Hanson, and A. C. Gossard, Rapid Single-Shot Measurement of a Singlet-Triplet Qubit, *Phys. Rev. Lett.* **103**, 160503 (2009).
- [39] J. I. Colless, A. C. Mahoney, J. M. Hornibrook, A. C. Doherty, H. Lu, A. C. Gossard, and D. J. Reilly, Dispersive Readout of a Few-Electron Double Quantum Dot with Fast rf Gate Sensors, *Phys. Rev. Lett.* **110**, 046805 (2013).
- [40] A. Cottet, C. Mora, and T. Kontos, Mesoscopic admittance of a double quantum dot, *Phys. Rev. B* **83**, 121311 (2011).
- [41] S. Schaal, I. Ahmed, J. A. Haigh, L. Hutin, B. Bertrand, S. Barraud, M. Vinet, C.-M. Lee, S. Stelmashenko, J. W. A. Robinson, J. Y. Qiu, S. Hacohen-Gourgy, I. Siddiqi, M. F. Gonzalez-Zalba, and J. J. L. Morton, Fast Gate-Based Readout of Silicon Quantum Dots Using Josephson Parametric Amplification, *Phys. Rev. Lett.* **124**, 067701 (2020).
- [42] B. Patra, R. M. Incandela, J. P. G. van Dijk, H. A. R. Homulle, L. Song, M. Shahmohammadi, R. B. Staszewski, A. Vladimirescu, M. Babaie, F. Sebastian, and E. Charbon, Cryo-cmos circuits and systems for quantum computing applications, *IEEE J. Solid-State Circuits* **53**, 309 (2018).